

Chapter 2

Representation of Atomic Environments

2.1 Introduction

The quantitative representation of atomic environments is an important tool in modern computational chemistry and condensed matter physics. For example, in structure search applications [1], each configuration that is found during the procedure depends numerically on the precise initial conditions and the path of the search, so it is important to be able to identify equivalent structures or detect similarities. In other applications, such as molecular dynamics simulation of phase transitions [2], one needs good order parameters capable of detecting changes in the local order around the atoms. In constructing interatomic potentials [3], the functional forms depend on elements of a carefully chosen representation of atomic neighbourhoods, e.g. bond lengths, bond angles, etc.

Although the Cartesian coordinate system provides a simple and unequivocal description of atomic systems, comparisons of structures based on it are difficult: the list of coordinates can be ordered arbitrarily, or two structures might be mapped to each other by a rotation, reflection or translation. Hence, two different lists of atomic coordinates can in fact represent the same or very similar structures. In a good representation, permutational, rotational and translational symmetries are built in explicitly, i.e. the representation is *invariant* with respect to these symmetries, while retaining the faithfulness of the Cartesian coordinates. If a representation is *complete*, a one-to-one mapping is obtained between the genuinely different atomic environments and the set of invariants comprising the representation.

The most well known invariants describing atomic neighbourhoods are the set of bond-order parameters proposed by Steinhardt et al. [4]. These have been successfully used as order parameters in studies of nucleation [5], phase transitions [6] and glasses [7]. In the following sections we show that the bond-order parameters actually form a subset of a more general set of invariants called the bispectrum. We prove that the bispectrum components indeed form a rotational and permutational invariant representation of atomic environments. The formally

infinite array of bispectral invariants provide an almost complete set, and by truncating it one obtains representations whose sensitivity can be refined at will.

2.2 Translational Invariants

The concept of the power spectrum and the bispectrum was originally introduced by the signal processing community. In the analysis of periodic signals the absolute phase is often irrelevant and a hindering factor, for example, when comparing signals. The problem of eliminating the phase of a periodic function is very similar to the problem of creating a rotationally invariant representation of spatial functions. We show how the bispectrum of periodic functions can be defined and discuss its possible uses in atomistic simulations.

2.2.1 Spectra of Signals

A periodic signal $f(t)$ (or a function defined on the circumference of a circle) where $t \in [0, 2\pi)$, can be represented by its Fourier series:

$$f(t) = \sum_n f_n \exp(i\omega_n t), \quad (2.1)$$

where the coefficients, f_n , can be obtained as follows:

$$f_n = \frac{1}{2\pi} \int_0^{2\pi} f(t) \exp(-i\omega_n t) dt. \quad (2.2)$$

A phase shift of the signal (or rotation of the function) by t_0 transforms the original signal according to

$$f(t) \rightarrow f(t + t_0), \quad (2.3)$$

and the coefficients become

$$f_n \rightarrow \exp(i\omega_n t_0) f_n. \quad (2.4)$$

It follows that the power spectrum of the signal defined as

$$p_n = f_n^* f_n \quad (2.5)$$

is invariant to such phase shifts:

$$p_n = f_n^* f_n \rightarrow (f_n \exp(i\omega_n t_0))^* (f_n \exp(i\omega_n t_0)) = f_n^* f_n, \quad (2.6)$$

Fig. 2.1 Two different periodic functions that share the same power spectrum coefficients

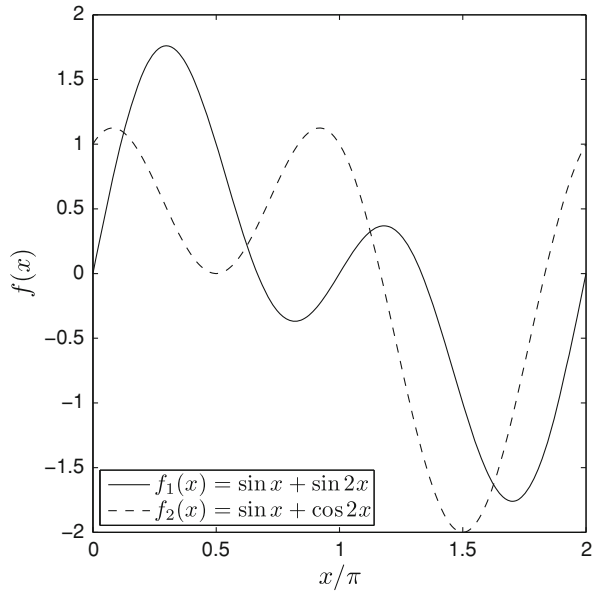


Table 2.1 Fourier and power spectrum coefficients of f_1 and f_2

ω	-2	-1	0	1	2
\mathbf{f}_1	$-i$	$-i$	0	i	i
\mathbf{f}_2	1	$-i$	0	i	1
$\mathbf{p}_1 = \mathbf{p}_2$	1	1	0	1	1

but the information content of different channels becomes decoupled. Figure 2.1 and Table 2.1 demonstrate two functions, $f_1 = \sin(t) + \sin(2t)$ and $f_2 = \sin(t) + \cos(2t)$, that can both be represented by the same power spectrum.

2.2.2 Bispectrum

As the power spectrum is not complete, i.e. the original function cannot be reconstructed from it, there is a need for an invariant representation from which the original function can (at least in theory) be restored. The bispectrum contains the relative phase of the different channels, moreover, it has been proven to be complete [8].

A periodic function $f : \mathbb{R}^n \rightarrow \mathbb{C}$, whose period is L_i in the i th direction, can be expressed in terms of a Fourier series:

$$f(\mathbf{r}) = \sum_{\omega} f(\omega) \exp(i\omega \mathbf{r}), \tag{2.7}$$

where the Fourier-components can be obtained from

$$f(\boldsymbol{\omega}) = \prod_{i=1}^n \frac{1}{L_i} \int_V f(\mathbf{r}) \exp(i\boldsymbol{\omega}\mathbf{r}) d\mathbf{r} \quad (2.8)$$

and $\boldsymbol{\omega} = (\omega_1, \omega_2, \dots, \omega_n)$. An arbitrary translation $\hat{T}(\mathbf{r}_0)$ transforms f as $f(\mathbf{r}) \rightarrow f(\mathbf{r} - \mathbf{r}_0)$, thus the Fourier-coefficients change as $f(\boldsymbol{\omega}) \rightarrow \exp(-i\boldsymbol{\omega}\mathbf{r}_0)f(\boldsymbol{\omega})$. The bispectrum of f is defined as the triple-correlation of the Fourier coefficients:

$$b(\boldsymbol{\omega}_1, \boldsymbol{\omega}_2) = f(\boldsymbol{\omega}_1)f(\boldsymbol{\omega}_2)f(\boldsymbol{\omega}_1 + \boldsymbol{\omega}_2)^*. \quad (2.9)$$

The bispectrum is invariant to translations:

$$\begin{aligned} b(\boldsymbol{\omega}_1, \boldsymbol{\omega}_2) &\rightarrow f(\boldsymbol{\omega}_1) \exp(i - \boldsymbol{\omega}_1 \mathbf{r}_0) f(\boldsymbol{\omega}_2) \exp(i - \boldsymbol{\omega}_2 \mathbf{r}_0) \\ &\times f(\boldsymbol{\omega}_1 + \boldsymbol{\omega}_2)^* \exp(i(\boldsymbol{\omega}_1 + \boldsymbol{\omega}_2) \mathbf{r}_0) = b(\boldsymbol{\omega}_1, \boldsymbol{\omega}_2). \end{aligned} \quad (2.10)$$

The bispectrum has been shown to be complete [8]. The proof, which is highly technical and would be too long to reproduce here is based on Group Theory. Further, Dianat and Raghuveer [9] proved that in case of one- and two-dimensional functions the original function can be restored using only the diagonal elements of the bispectrum, i.e. only the components for which $\boldsymbol{\omega}_1 = \boldsymbol{\omega}_2$.

2.2.3 Bispectrum of Crystals

Crystals are periodic repetitions of a unit cell in space in each of the three directions defined by the lattice vectors. A unit cell can be described as a parallelepiped (the description used by the conventional Bravais system of lattices) containing some number of atoms at given positions. The three independent edges of the parallelepiped are the lattice vectors, whereas the positions of the atoms in the unit cell form the basis. Defining crystals in this way is not unique, as any subset of a crystal which generates it by translations can be defined as a unit cell, for example, a Wigner–Seitz cell, which is not even necessarily a parallelepiped.

Thus a crystal can be described by the coordinates of the basis atoms \mathbf{r}_i , where $i = 1, \dots, N$ and the three lattice vectors $\mathbf{a}_\alpha, \alpha = 1, 2, 3$. The position of the basis can be given in terms of the fractional coordinates \mathbf{x}_i , such that

$$\mathbf{r}_i = \sum_{\alpha=1}^3 x_{i\alpha} \mathbf{a}_\alpha, \quad (2.11)$$

where $0 < x_{i\alpha} < 1$.

In the same way as in the case of atomic environments, the order of the atoms in the basis is arbitrary. We introduce the permutational invariance through the atomic density:

$$\rho(\mathbf{x}) = \sum_i \delta(\mathbf{x} - \mathbf{x}_i). \quad (2.12)$$

ρ is a periodic function in the unit cube, therefore we can expand it in a Fourier series and calculate invariant features such as the power spectrum and bispectrum. It can be noted that the power spectrum of ρ is equivalent to the structure factor used in X-ray and neutron diffraction, and it is clear from Sect. 2.2.1 why the structure factor is not sufficient to determine the exact structure of a crystal. In contrast, the bispectrum of the atomic density function could be used as a unique fingerprint of the crystal that is invariant to the permutation and translation of the basis.

We note that permuting the lattice vectors of the crystal permutes the reciprocal lattice vectors which therefore, mixes the elements of the bispectrum. This problem can be eliminated by first matching the lattice vectors of the two structures which are being compared. The rotation of the entire lattice does not change the fractional coordinates, hence the bispectrum is invariant to global rotations.

2.3 Rotationally Invariant Features

Invariant features of atomic environments can be constructed by several methods, of which we list a few here. In interatomic potentials, a set of geometric parameters are used, such as bond lengths, bond angles and tetrahedral angles. These are rotationally invariant by construction, but the size of a complete set of such parameters grows as $\exp(N)$, where N is the number of neighbours. The complete set is vastly redundant, but there is no systematic way of reducing the number of parameters without losing completeness.

A more compact rotationally invariant representation of the atomic environment can be built in the form of a matrix by using the bond vectors $\mathbf{r}_i, i = 1, \dots, N$ between the central atom and its N neighbours. The elements of the matrix are given by the dot product

$$M_{ij} = \mathbf{r}_i \cdot \mathbf{r}_j. \quad (2.13)$$

Matrix \mathbf{M} contains the bond lengths on its diagonal, whereas the off-diagonal elements are related to the bond angles. It can be shown that \mathbf{M} is a complete representation [10]. However, permuting the neighbouring atoms shuffles the columns and rows of \mathbf{M} , thus \mathbf{M} is not a suitable invariant representation.

Permutational invariance can be achieved by using the symmetric polynomials [11]. These are defined by

$$\Pi_k(x_1, x_2, \dots, x_N) = \Pi_k(x_{\pi_1}, x_{\pi_2}, \dots, x_{\pi_N}) \quad (2.14)$$

for every π , where π is an arbitrary permutation of the vector $(1, 2, \dots, N)$. The first three symmetric polynomials are

$$\Pi_1(x_1, x_2, \dots, x_N) = \sum_i^N x_i \quad (2.15)$$

$$\Pi_2(x_1, x_2, \dots, x_N) = \sum_{i < j}^N x_i x_j \quad (2.16)$$

$$\Pi_3(x_1, x_2, \dots, x_N) = \sum_{i < j < k}^N x_i x_j x_k. \quad (2.17)$$

The series of polynomials form a complete representation, however, this set is not rotationally invariant.

2.3.1 Bond-order Parameters

As a first step to derive a more general invariant representation of atomic environments, we define the local atomic density as

$$\rho_i(\mathbf{r}) = \sum_j \delta(\mathbf{r} - \mathbf{r}_{ij}), \quad (2.18)$$

where the index j runs over the neighbours of atom i . The local atomic density is already invariant to permuting neighbours, as changing the order of the atoms in the neighbour list only affects the order of the summation. This function could be expanded in terms of spherical harmonics (dropping the atomic index i for clarity):

$$\rho(\mathbf{r}) = \sum_{l=0}^l \sum_{m=-l}^l c_{lm} Y_{lm}(\theta(\mathbf{r}), \phi(\mathbf{r})). \quad (2.19)$$

However, we should note that this representation does not contain information about the distances of neighbours. In fact, $\rho(\mathbf{r})$ represented this way is the projection of the positions of neighbouring atoms onto the unit sphere. The properties of functions defined on the unit sphere are described by the group theory of $\text{SO}(3)$, the group of rotations about the origin.

The spherical harmonics functions form an orthonormal basis set for L_2 :

$$\langle Y_{lm} | Y_{l'm'} \rangle = \delta_{ll'} \delta_{mm'}, \quad (2.20)$$

where the inner product of functions f and g is defined as

$$\langle f | g \rangle = \int f^*(\mathbf{r}) g(\mathbf{r}) d\mathbf{r}. \quad (2.21)$$

The coefficients c_{lm} can be determined as

$$c_{lm} = \langle \rho | Y_{lm} \rangle = \sum_j Y_{lm}(\theta(\mathbf{r}_{ij}), \phi(\mathbf{r}_{ij})). \quad (2.22)$$

We note that the order parameters Q_{lm} introduced by Steinhardt et al. [4] are proportional to the coefficients c_{lm} . In their work, they defined the bonds in the system as vectors joining neighbouring atoms. Defining which atoms are the neighbours of a particular atom can be done by using a simple distance cutoff or via the Voronoi analysis. Once the set of neighbours has been defined, each bond \mathbf{r}_{ij} connecting neighbour atoms i and j is represented by a set of spherical harmonics coefficients

$$Y_{lm}(\hat{\mathbf{r}}_{ij}) = Y_{lm}(\theta(\mathbf{r}_{ij}), \phi(\mathbf{r}_{ij})). \quad (2.23)$$

Averaging the coefficients for atom i provides the atomic order parameters for that atom

$$Q_{lm}^i = \frac{1}{N_i} \sum_j Y_{lm}(\hat{\mathbf{r}}_{ij}), \quad (2.24)$$

where N_i is the number of neighbours of atom i . Similarly, averaging over all bonds in the system gives a set of global order parameters

$$\bar{Q}_{lm} = \frac{1}{N_b} \sum_{ij} Y_{lm}(\hat{\mathbf{r}}_{ij}), \quad (2.25)$$

where N_b is the total number of bonds. Both of these order parameters are invariant to permutations of atoms and to translations, but they still depend on the orientation of the reference frame. However, rotationally invariant combinations of these order parameters can be constructed as follows:

$$Q_l^i = \left(\frac{4\pi}{2l+1} \sum_{m=-l}^l (Q_{lm}^i)^* Q_{lm}^i \right)^{1/2} \quad \text{and} \quad (2.26)$$

$$W_l^i = \sum_{m_1, m_2, m_3=-l}^l \begin{pmatrix} l & l & l \\ m_1 & m_2 & m_3 \end{pmatrix} Q_{lm_1}^i Q_{lm_2}^i Q_{lm_3}^i \quad (2.27)$$

for atoms and

$$\bar{Q}_l = \left(\frac{4\pi}{2l+1} \sum_{m=-l}^l \bar{Q}_{lm}^* \bar{Q}_{lm} \right)^{1/2} \quad (2.28)$$

$$\bar{W}_l = \sum_{m_1, m_2, m_3=-l}^l \begin{pmatrix} l & l & l \\ m_1 & m_2 & m_3 \end{pmatrix} \bar{Q}_{lm_1} \bar{Q}_{lm_2} \bar{Q}_{lm_3} \quad (2.29)$$

for global structures. The factor in parentheses is the Wigner-3jm symbol, which is nonzero only for $m_1 + m_2 + m_3 = 0$.

Q_l^i and W_l^i are called second-order and third-order bond-order parameters, respectively. It is possible to normalise W_l^i such that it does not depend strongly on the number of neighbours as follows:

$$\hat{W}_l^i = W_l^i / \left(\sum_{m=-l}^l (Q_{lm}^i)^* Q_{lm}^i \right)^{3/2}. \quad (2.30)$$

Bond-order parameters were originally introduced by Steinhardt et al. [4] for studying the order in liquids and glasses, but their approach was adopted soon for a wide range of applications. For example, the bond-order parameters, when averaged over all bonds in the system, can be used as reaction coordinates in phase transitions [12].

For symmetry reasons, bond order parameters with $l \geq 4$ have non-zero values in clusters with cubic symmetry and $l \geq 6$ for clusters with icosahedral symmetry. The most widely calculated bond order parameters are $l = 4$ and $l = 6$. Different values correspond to crystalline materials with different symmetry, while the global values vanish in disordered phases, such as in liquids. This feature made the Q and W invariants attractive for use as bond order parameters in many applications.

2.3.2 Power Spectrum

Using some basic concepts from representation theory, we can now prove that the second-order invariants are rotationally invariant, then we show a more general form of invariants, a superset consisting of third-order invariants [13]. An arbitrary rotation \hat{R} operating on a spherical harmonic function Y_{lm} transforms it into a linear combination of spherical harmonics with the same l index:

$$\hat{R}Y_{lm} = \sum_{m'=-l}^l D_{mm'}^{(l)}(R)Y_{lm'}, \quad (2.31)$$

where the matrices $\mathbf{D}^{(l)}(R)$ are also known as the Wigner-matrices. The elements of the Wigner matrices can be generated by

$$D_{mm'}^{(l)}(R) = \langle Y_{lm} | \hat{R} | Y_{lm'} \rangle. \quad (2.32)$$

It follows that the rotation operator \hat{R} acts on the function ρ as

$$\begin{aligned} \hat{R}\rho &= \hat{R} \sum_{l=0}^{\infty} \sum_{m=-l}^l c_{lm} Y_{lm} = \sum_{l=0}^{\infty} \sum_{m=-l}^l c_{lm} \hat{R}Y_{lm} \\ &= \sum_{l=0}^{\infty} \sum_{m=-l}^l \sum_{m'=-l}^l c_{lm} D_{mm'}^{(l)}(R) Y_{lm'} \\ &= \sum_{l=0}^{\infty} \sum_{m'=-l}^l c'_{lm'} Y_{lm'}, \end{aligned} \quad (2.33)$$

thus the vector of coefficients \mathbf{c}_l transform under rotation as

$$\mathbf{c}_l \rightarrow \mathbf{D}^{(l)}(R)\mathbf{c}_l. \quad (2.34)$$

Making use of the fact that rotations are unitary operations, it is possible to show that the matrices $\mathbf{D}^{(l)}$ are unitary, i.e.

$$\left(\mathbf{D}^{(l)}\right)^\dagger \mathbf{D}^{(l)} = \mathbf{I}, \quad (2.35)$$

leading us to a set of rotationally invariant coefficients, the rotational power spectrum:

$$p_l = \mathbf{c}_l^\dagger \mathbf{c}_l. \quad (2.36)$$

The coefficients of the power spectrum remain invariant under rotations:

$$p_l = \mathbf{c}_l^\dagger \mathbf{c}_l \rightarrow \left(\mathbf{c}_l^\dagger \left(\mathbf{D}^{(l)}\right)^\dagger\right) \left(\mathbf{D}^{(l)} \mathbf{c}_l\right) = \mathbf{c}_l^\dagger \mathbf{c}_l. \quad (2.37)$$

It can be directly seen that the second-order bond-order parameters are related to the power spectrum via the simple equation

$$Q_l = \left(\frac{4\pi}{2l+1} p_l\right)^{1/2}. \quad (2.38)$$

The power spectrum is a very impoverished representation of the original function ρ , because all p_l coefficients are rotationally invariant *independently*, i.e. different l channels are decoupled. This representation, although rotationally invariant, is, in turn, severely incomplete.

The incompleteness of the power spectrum can be demonstrated by the following example. Assuming a function f in the form

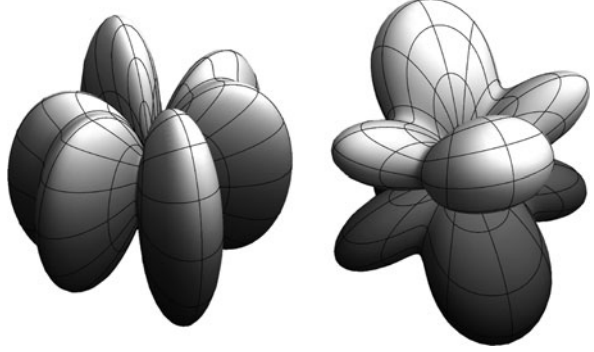
$$f(\hat{\mathbf{r}}) = \sum_{m=-l_1}^{l_1} \alpha_m Y_{l_1 m}(\hat{\mathbf{r}}) + \sum_{m=-l_2}^{l_2} \beta_m Y_{l_2 m}(\hat{\mathbf{r}}), \quad (2.39)$$

its power spectrum elements are $p_{l_1} = |\boldsymbol{\alpha}|^2$ and $p_{l_2} = |\boldsymbol{\beta}|^2$. Thus only the *length* of the vectors $\boldsymbol{\alpha}$ and $\boldsymbol{\beta}$ are constrained by the power spectrum, their relative orientation is lost, i.e. the information content of channels l_1 and l_2 becomes decoupled. Figure 2.2 shows two different angular functions, $f_1 = Y_{22} + Y_{2-2} + Y_{33} + Y_{3-3}$ and $f_2 = Y_{21} + Y_{2-1} + Y_{32} + Y_{3-2}$ that have the same power spectrum $p_2 = 2$ and $p_3 = 2$.

2.3.3 Bispectrum

We will now generalise the concept of the power spectrum in order to obtain a more complete set of invariants via the coupling of the different angular

Fig. 2.2 Two different angular functions that share the same power spectrum coefficients



momentum channels [13]. Let us consider the direct product $\mathbf{c}_{l_1} \otimes \mathbf{c}_{l_2}$, which transforms under a rotation as

$$\mathbf{c}_{l_1} \otimes \mathbf{c}_{l_2} \rightarrow \left(\mathbf{D}^{(l_1)} \otimes \mathbf{D}^{(l_2)} \right) (\mathbf{c}_{l_1} \otimes \mathbf{c}_{l_2}). \quad (2.40)$$

It follows from the representation theory of groups that the direct product of two irreducible representations can be decomposed into direct sum of irreducible representations of the same group. In case of the $\text{SO}(3)$ group, the direct product of two Wigner-matrices can be decomposed into a direct sum of Wigner-matrices in the form

$$\mathbf{D}^{(l_1)} \otimes \mathbf{D}^{(l_2)} = (\mathbf{C}^{l_1, l_2})^\dagger \left[\bigoplus_{l=|l_1-l_2|}^{l_1+l_2} \mathbf{D}^{(l)} \right] \mathbf{C}^{l_1, l_2}, \quad (2.41)$$

where \mathbf{C}^{l_1, l_2} denote the Clebsch–Gordan coefficients. The matrices of Clebsch–Gordan coefficients are themselves unitary, hence the vector $\mathbf{C}^{l_1, l_2}(\mathbf{c}_{l_1} \otimes \mathbf{c}_{l_2})$ transforms as

$$\mathbf{C}^{l_1, l_2}(\mathbf{c}_{l_1} \otimes \mathbf{c}_{l_2}) \rightarrow \left[\bigoplus_{l=|l_1-l_2|}^{l_1+l_2} \mathbf{D}^{(l)} \right] \mathbf{C}^{l_1, l_2}(\mathbf{c}_{l_1} \otimes \mathbf{c}_{l_2}). \quad (2.42)$$

We define $\mathbf{g}_{l_1, l_2, l}$ as

$$\bigoplus_{l=|l_1-l_2|}^{l_1+l_2} \mathbf{g}_{l_1, l_2, l} \equiv \mathbf{C}^{l_1, l_2}(\mathbf{c}_{l_1} \otimes \mathbf{c}_{l_2}), \quad (2.43)$$

i.e. the $\mathbf{g}_{l_1, l_2, l}$ is that part of the RHS which transforms under rotation as

$$\mathbf{g}_{l_1, l_2, l} \rightarrow \mathbf{D}^{(l)} \mathbf{g}_{l_1, l_2, l}. \quad (2.44)$$

Analogously to the power spectrum, the bispectrum components or cubic invariants, can be written as

$$b_{l_1, l_2, l} = \mathbf{c}_l^\dagger \mathbf{g}_{l_1, l_2, l}, \quad (2.45)$$

which are invariant to rotations:

$$b_{l_1, l_2, l} = \mathbf{c}_l^\dagger \mathbf{g}_{l_1, l_2, l} \rightarrow \left(\mathbf{c}_l \mathbf{D}^{(l)} \right)^\dagger \mathbf{D}^{(l)} \mathbf{g}_{l_1, l_2, l} = \mathbf{c}_l^\dagger \mathbf{g}_{l_1, l_2, l} \quad (2.46)$$

Kondor showed that the bispectrum of the $\text{SO}(3)$ space is not complete, i.e. the bispectrum does not determine uniquely the original function. This is a deficiency due to the fact that the unit sphere, S_2 is a homogeneous space. However, he states that the bispectrum is still a remarkably rich invariant representation of the function.

Rewriting the bispectrum formula as

$$b_{l_1, l_2, l} = \sum_{m=-l}^l \sum_{m_1=-l_1}^{l_1} \sum_{m_2=-l_2}^{l_2} c_{lm}^* C_{l_1 m_1 l_2 m_2}^{lm} c_{l_1 m_1} c_{l_2 m_2}, \quad (2.47)$$

the similarity to the third-order bond-order parameters becomes apparent. Indeed, the Wigner 3jm-symbols are related to the Clebsch–Gordan coefficients through

$$\begin{pmatrix} l_1 & l_2 & l_3 \\ m_1 & m_2 & m_3 \end{pmatrix} = \frac{(-1)^{l_1 - l_2 - m_3}}{\sqrt{2l_3 + 1}} C_{l_1 m_1 l_2 m_2}^{l_3 m_3}. \quad (2.48)$$

For the spherical harmonics $Y_{lm} = (-1)^m Y_{l-m}^*$, thus the third-order parameters W_l are simply the diagonal elements of the bispectrum $b_{l,l,l}$ up to a scalar factor, and thus, the bispectrum is a superset of the third-order bond-order parameters. Further, considering that $Y_{00} \equiv 1$, therefore the coefficient c_{00} is simply the number of neighbours N , and $C_{m,0,m_2}^{l,0,l_2} = \delta_{l,l_2} \delta_{m,m_2}$, we notice that the bispectrum elements $l_1 = 0, l = l_2$ are the power spectrum components, previously introduced:

$$b_{l,0,l} = N_i \sum_{m=-l}^l \sum_{m_2=-l}^l c_{lm}^* \delta_{m,m_2} c_{lm_2} = N_i \sum_{m=-l}^l c_{lm}^* c_{lm} = N_i p_l. \quad (2.49)$$

Finally, the relationship between the bond-order parameters and the bispectrum can be summarised as

$$Q_l \propto \sqrt{p_l} \propto \sqrt{b_{l,0,l}} \quad (2.50)$$

$$W_l \propto b_{l,l,l}. \quad (2.51)$$

2.3.3.1 Radial Dependence

The bispectrum is still a very incomplete representation, as it uses the unit-sphere projection of the atomic environment, i.e. the distance of the atoms from the centre

is not represented. One way to improve this shortcoming—namely, the lack of radial information—is to introduce radial basis functions [14], completing the basis for three-dimensional space. In Eq. 2.19, we use the product of spherical harmonics and a linearly independent set of radial functions g_n :

$$\rho(\mathbf{r}) = \sum_n \sum_{l=0} \sum_{m=-l}^l c_{nlm} g_n(r) Y_{lm}(\theta(\mathbf{r}), \phi(\mathbf{r})). \quad (2.52)$$

If the set of radial basis functions is not orthonormal, i.e. $\langle g_n | g_m \rangle = S_{nm} \neq \delta_{nm}$, after obtaining the coefficients c'_{nlm} with

$$c'_{nlm} = \langle g_n Y_{lm} | \rho \rangle, \quad (2.53)$$

the elements c_{nlm} are given as

$$c_{nlm} = \sum_{n'} (S^{-1})_{n'n} c'_{n'lm}. \quad (2.54)$$

In practice, when constructing the invariants, both c'_{nlm} and c_{nlm} can be used.

Rotational invariance only applies globally, therefore the different angular momentum channels corresponding to various radial basis functions need to be coupled. Simply extending Eq. 2.47 to the form

$$b_{n,l_1,l_2,l} = \sum_{m=-l}^l \sum_{m_1=-l_1}^{l_1} \sum_{m_2=-l_2}^{l_2} c_{nlm}^* C_{l_1 m_1 l_2 m_2}^{lm} c_{nl_1 m_1} c_{nl_2 m_2}, \quad (2.55)$$

provides a set of invariants describing the three-dimensional neighbourhood of the atom. In fact, this formula can easily lead to a poor representation, if the radial functions have little overlap with each other, as the coefficients belonging to different n channels become decoupled. To avoid this, it is necessary to choose wide, overlapping radial functions, although this greatly reduces the sensitivity of each channel (Fig. 2.3). The fine-tuning of the basis set is rather arbitrary, and there does not necessarily exist an optimum for all systems. An alternative way to construct invariants from \mathbf{c} is to couple different radial channels, for example, as

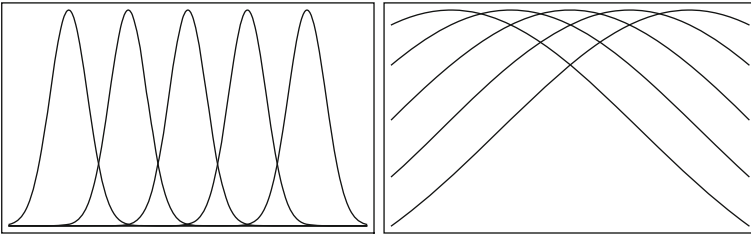


Fig. 2.3 Two possible sets of radial basis functions, Gaussians centred at different radii. The narrow Gaussians are more sensitive to changes in radial positions, but the coupling between them is weaker

$$b_{n_1, n_2, l_1, l_2, l} = \sum_{m=-l}^l \sum_{m_1=-l_1}^{l_1} \sum_{m_2=-l_2}^{l_2} c_{n_1 l m}^* C_{l_1 m_1 l_2 m_2}^{l m} c_{n_2 l_1 m_1} c_{n_2 l_2 m_2}. \quad (2.56)$$

Now we ensure that radial channels cannot become decoupled, but at the price of increasing the number of invariants quadratically. Although adding a suitable set of radial functions allows one to construct a complete representation, we found this approach overly complicated. A high degree of arbitrariness is introduced by having to choose a radial basis.

2.3.4 4-Dimensional Bispectrum

Instead of using a rather arbitrary radial basis set, we propose a generalisation of the power spectrum and bispectrum that does not require the explicit introduction of a radial basis set, yet still forms a complete basis of three-dimensional space. We start by projecting the atomic neighbourhood density onto the surface of the four-dimensional unit sphere, in a similar fashion to the Riemann-construction:

$$\mathbf{r} \equiv \begin{pmatrix} x \\ y \\ z \end{pmatrix} \rightarrow \begin{cases} \phi = \arctan(y/x) \\ \theta = \arccos(z/|\mathbf{r}|), \\ \theta_0 = |\mathbf{r}|/r_0 \end{cases}, \quad (2.57)$$

where $r_0 > r_{\text{cut}}/\pi$. Using this projection, rotations in the three-dimensional space correspond to rotations in the four-dimensional space. Figure 2.4 shows such projections for one and two dimensions, which can be more easily drawn than the three-dimensional case that we use here.

An arbitrary function ρ defined on the surface of a 4D sphere can be numerically represented using the hyperspherical harmonics functions $U_{m'm}^j(\phi, \theta, \theta_0)$:

$$\rho = \sum_{j=0}^{\infty} \sum_{m, m'=-j}^j c_{m'm}^j U_{m'm}^j. \quad (2.58)$$

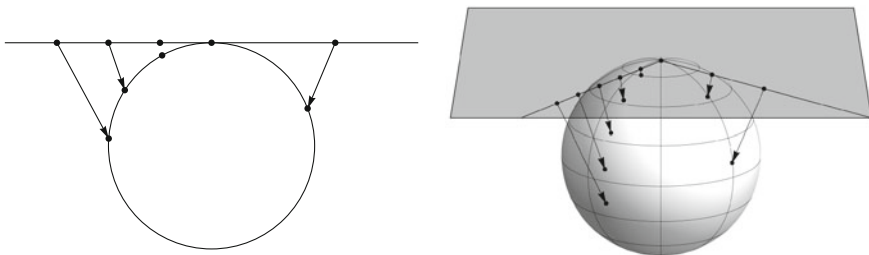


Fig. 2.4 Projection of a line to a circle (*left*), projection the two-dimensional plane onto the three-dimensional sphere (*right*). The projection we use is in Eq. 2.57 the generalisation to one more dimension

The hyperspherical harmonics form an orthonormal basis set, thus the expansion coefficients $c_{m'm}^j$ can be calculated via

$$c_{m'm}^j = \langle U_{m'm}^j | \rho \rangle, \quad (2.59)$$

where $\langle \cdot | \cdot \rangle$ denotes the inner product in four-dimensional space. Although the coefficients $c_{m'm}^j$ have two indices for each j , they are vectors and, for clarity, we denote them as \mathbf{c}^j . Similarly to the three-dimensional case, a unitary operation \hat{R} , such as a rotation, acts on the hyperspherical harmonics functions as

$$\hat{R} U_{m'_1 m_1}^j = \sum_{m'_2 m_2} R_{m'_1 m_1 m'_2 m_2}^j U_{m'_2 m_2}^j, \quad (2.60)$$

where the matrix elements $R_{m'_1 m_1 m'_2 m_2}^j$ are given by

$$R_{m'_1 m_1 m'_2 m_2}^j = \langle U_{m'_1 m_1}^j | \hat{R} | U_{m'_2 m_2}^j \rangle. \quad (2.61)$$

Hence the rotation \hat{R} acting on ρ transforms the coefficient vectors \mathbf{c}^j according to

$$\mathbf{c}^j \rightarrow \mathbf{R}^j \mathbf{c}^j. \quad (2.62)$$

\mathbf{R}^j are unitary matrices, i.e. $(\mathbf{R}^j)^\dagger \mathbf{R}^j = \mathbf{I}$.

The product of two hyperspherical harmonics functions can be expressed as the linear combination of hyperspherical harmonics [15]:

$$U_{m'_1 m_1}^{l_1} U_{m'_2 m_2}^{l_2} = \sum_{l=|l_1-l_2|}^{l_1+l_2} C_{l_1 m_1 l_2 m_2}^{lm} C_{l_1 m_1 l_2 m_2}^{lm} U_{m' m}^l, \quad (2.63)$$

where $C_{l_1 m_1 l_2 m_2}^{lm}$ are the well-known Clebsch–Gordan coefficients. We can recognise in Eq. 2.63 the four dimensional analogues of the Clebsch–Gordan expansion coefficients, defined as $H_{l_1 m_1 m'_1, l_2 m_2 m'_2}^{lm m'} \equiv C_{l_1 m_1 l_2 m_2}^{lm} C_{l_1 m'_1 l_2 m'_2}^{lm'}$. Using the matrix notation of the expansion coefficients, it can be shown that the direct product of the four-dimensional rotation matrices decompose according to

$$\mathbf{R}^{j_1} \otimes \mathbf{R}^{j_2} = (\mathbf{H}^{j_1 j_2})^\dagger \left[\bigoplus_{j=|j_1-j_2|}^{j_1+j_2} \mathbf{R}^j \right] \mathbf{H}^{j_1 j_2}. \quad (2.64)$$

The remainder of the derivation continues analogously to the 3D case. Finally, we arrive at the expression for the bispectrum elements, given by

$$B_{j_1 j_2 j} = \sum_{m'_1 m_1 = -j_1}^{j_1} \sum_{m'_2 m_2 = -j_2}^{j_2} \sum_{m' m = -j}^j (c_{m' m}^j)^* C_{j_1 m_1 j_2 m_2}^{jm} C_{j_1 m'_1 j_2 m'_2}^{jm'} c_{m'_1 m_1}^{j_1} c_{m'_2 m_2}^{j_2}. \quad (2.65)$$

Note that the 4D power spectrum can be constructed as

$$P_j = \sum_{m', m=-j}^j (c_{m'm}^j)^* c_{m'm}^j. \quad (2.66)$$

The 4D bispectrum is invariant with respect to rotations of four-dimensional space, which include three-dimensional rotations. However, there are additional rotations, associated with the third polar angle θ_0 , which, in our case, represents the radial information. In order to eliminate the invariance with respect to the third polar angle, we modified the atomic density as follows:

$$\rho_i(\mathbf{r}) = \delta(\mathbf{0}) + \sum_j \delta(\mathbf{r} - \mathbf{r}_{ij}), \quad (2.67)$$

i.e. by adding the central atom as a reference point.

The magnitude of the elements of the bispectrum scale as the cube of the number of neighbours, so we take the cube-root of the coefficients in order to make the comparison of different spectra easier.

2.3.5 Results

In practice, the infinite spherical harmonic expansion of the atomic neighbourhood is truncated to obtain a finite array of bispectral invariants. In Fig. 2.5 we show the 4D bispectra of atoms in a variety of environments, truncated to $j \leq 4$, which gives 42 bispectrum coefficients. In each case the r_0 parameter was set to highlight differences between the bispectral elements.

It can be seen from Fig. 2.5 that the bispectrum is capable of distinguishing very subtle differences in atomic neighbourhood environments. Some points of particular interest are the following. The difference between the face-centred cubic (fcc) and the hexagonal close-packed (hcp) structures is very small within the first neighbour shell, as is the difference between the corresponding bispectra (panel a). However, the difference is much more pronounced once second neighbours are included (panel b). The difference between the cubic and hexagonal diamond lattices is the stacking order of the (111) sheets. The positions of the four nearest neighbours and nine atoms of the second-nearest neighbour shell are the same and, only the positions of the remaining three neighbours are different, as shown in Fig. 2.6. The curves in Fig. 2.5c reflect the similarity of these two structures: most of the bispectrum coefficients are equal, except a few, which can be used for distinguishing the structures. Figure 2.5d shows the bispectra of three atoms in perfect diamond lattices, which differ in the lattice constants. This plot illustrates the sensitivity of the bispectrum in the radial dimension because the expansion of a lattice leaves all angular coordinates the same. It can be seen that the first element of the bispectrum array remains the same, because this is proportional only to the number of neighbours.

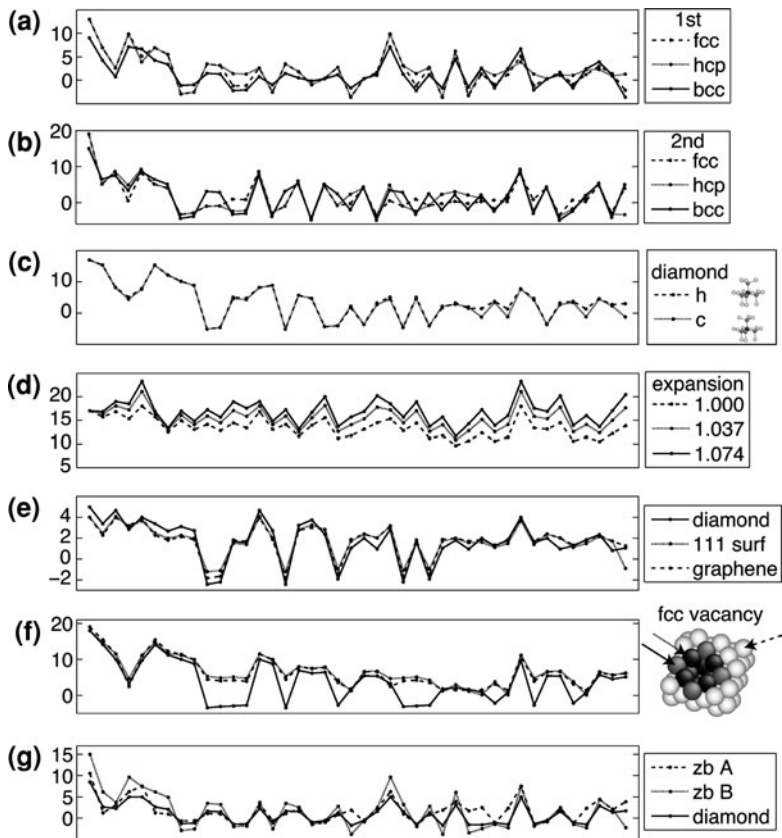
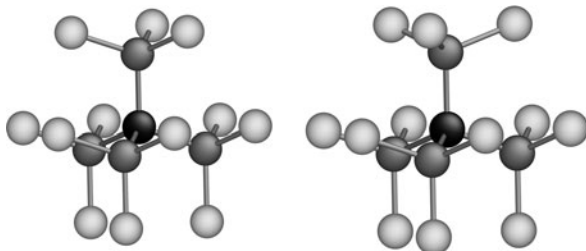


Fig. 2.5 Four-dimensional bispectra of atoms in various structures: **a** fcc/hcp/bcc lattices with a first neighbour cutoff; **b** fcc/hcp/bcc lattices with a second neighbour cutoff; **c** hexagonal and cubic diamond lattice; **d** expansion of a diamond lattice; **e** bulk diamond, (111) surface of diamond and graphene; **f** fcc vacancy; **g** the A and B atoms in a zincblende structure, compared with diamond

Fig. 2.6 Cubic and hexagonal diamond. Cubic diamond is shown in the *left*



We performed the principle component analysis [16] on the bispectra of atoms in a slab of silicon. On the surface of the slab, the atoms were arranged according to the 7×7 reconstruction [17]. The position of the atoms were randomised by

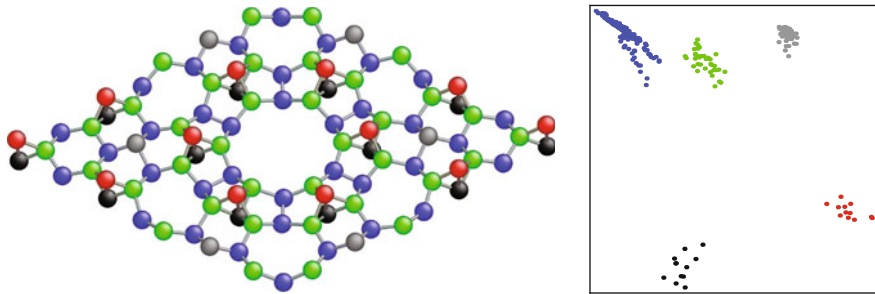


Fig. 2.7 Principle component analysis of the bispectrum of atoms on the 7×7 reconstruction of the (111) surface of silicon

0.3 Å. We projected the 42-dimensional space of the bispectrum—which corresponds to $j \leq 4$ —to the two-dimensional plane and clustered the points using the k-means algorithm [18]. In Fig. 2.7, we show the result of the principle component analysis. Different colours are assigned to each cluster identified by the k-means method, and we coloured the atoms with respect to the cluster they belong. This example demonstrates that the bispectrum can be used to identify atomic environments in an automatic way.

It is straightforward to describe multi-species atomic environments using the bispectrum. We modify the atomic density function defined in Eq. 2.18 as

$$\rho_i(\mathbf{r}) = s_i \delta(\mathbf{0}) + \sum_j s_j \delta(\mathbf{r} - \mathbf{r}_{ij}), \quad (2.68)$$

where \mathbf{s} contains an arbitrary set of coefficients, different for each species, which are thus distinguished. Figure 2.5g shows the resulting bispectra for the two different atoms in the zincblende lattice, as well as the diamond lattice for comparison. It can be seen that the bispectrum successfully distinguishes between the different species.

References

1. C.J. Pickard, R.J. Needs, *Nat. Mater.* **7**, 775 (2008)
2. D.J. Wales, *Energy Landscapes*. (Cambridge University Press, Cambridge, 2003)
3. J. Behler, M. Parrinello, *Phys. Rev. Lett.* **98**, 146401 (2007)
4. P.J. Steinhardt, D.R. Nelson, M. Ronchetti, *Phys. Rev. B* **28**, 784 (1983)
5. J.S. van Duijneveldt, D. Frenkel, *J. Chem. Phys.* **96**, 4655 (1992)
6. E.R. Hernández, J. Íñiguez, *Phys. Rev. Lett.* **98**, 055501 (2007)
7. A. van Blaaderen, P. Wiltzius, *Science* **270**, 1177 (1995)
8. R. Kakarala, *Triple Correlation on Groups*, Ph.D. thesis, Department of Mathematics, UC Irvine, 1992
9. S.A. Dianat, R.M. Rao, *Opt. Eng.* **29**, 504 (1990)
10. H. Weyl, *The Theory of Groups and Quantum Mechanics*. (Methuen, London, 1931)

11. P. Borwein, T. Erdélyi, *Polynomials and Polynomial Inequalities*. (Springer, New York, 1995)
12. D. Moroni, P.R. ten Wolde, P.G. Bolhuis, Phys. Rev. Lett. **94**, 235703 (2005)
13. R. Kondor, <http://arxiv.org/abs/cs.CV/0701127>, 2007
14. C.D. Taylor, Phys. Rev. B **80**, 024104 (2009)
15. D.A. Varshalovich, A.N. Moskalev, V.K. Khersonskii, Quantum Theory of Angular Momentum (World Scientific, Teaneck, 1987)
16. K. Pearson, Phil. Mag. **2**, 559 (1901)
17. K.C. Pandey, Physica **117**, **118**, 761 (1983)
18. A.K. Jain, M.N. Murty, P.J. Flynn, ACM Comp. Surv. **31**, 264 (2000)

<http://www.springer.com/978-3-642-14066-2>

The Gaussian Approximation Potential
An Interatomic Potential Derived from First Principles
Quantum Mechanics

Bartók-Pártay, A.

2010, XIV, 90 p. 31 illus., 2 illus. in color., Hardcover

ISBN: 978-3-642-14066-2